ORIGINAL PAPER

CrossMark

Functional properties and electrochemical performance of Ca-doped $Sr_{2-x}Ca_xFe_{1.5}Mo_{0.5}O_{6-\delta}$ as anode for solid oxide fuel cells

Denis A. Osinkin [1,2] · S. M. Beresnev [1] · A. V. Khodimchuk [1,2] · I. V. Korzun [1] · N. I. Lobachevskaya [3] · A. Yu Suntsov [3]

Abstract

Performance of Ca-doped strontium ferrite-molybdate $Sr_{2-x}Ca_xFe_{1.5}Mo_{0.5}O_{6-\delta}$ ($x = 0, 0.05, 0.15, 0.3, 0.5$) has been studied under reducing conditions. Thermogravimetry (TG) analysis in 5% H_2/Ar and DSC measurements in high-purity argon demonstrated that the compositions are highly stable and there are no phase transitions. The best electrochemical and electrical performances of about 0.12 Ω cm^2 and 33 S/cm at 800 °C in wet hydrogen, respectively, were obtained for the $Sr_{1.85}Ca_{0.15}Fe_{1.5}Mo_{0.5}O_{6-\delta}$ anode. The EIS spectra were analyzed by means of distribution relaxation times and non-linear least squares methods, which made it possible to determine the behavior of the rate-limiting steps of hydrogen oxidation. Solid oxide fuel cells (SOFC) of planar design with the 1.5 mm LaGaO$_3$-based supporting electrolyte, with the $Sr_{1.85}Ca_{0.15}Fe_{1.5}Mo_{0.5}O_{6-\delta}$ symmetrical electrodes and with the $Sr_{2-x}Ca_xFe_{1.5}Mo_{0.5}O_{6-\delta}$ ($x = 0.15$ and 0.3) anode and the 70 wt% $Pr_{0.9}Y_{0.1}BaCo_2O_{6-\delta}$ + 30 wt% SDC cathode have been studied. The obtained results demonstrated a low anode overvoltage, which was about 0.12 V at 1 A/cm^2 and 800 °C in wet hydrogen. The maximum power density of SOFC with the $Sr_{1.85}Ca_{0.15}Fe_{1.5}Mo_{0.5}O_{6-\delta}$ anode and cobaltite cathode was about 0.18 W/cm^2 at 800 °C under air/wet hydrogen conditions. The obtained results elucidate that $Sr_{1.85}Ca_{0.15}Fe_{1.5}Mo_{0.5}O_{6-\delta}$ is a promising anode for solid oxide fuel cells.

Keywords Ca-doped $Sr_{2-x}Ca_xFe_{1.5}Mo_{0.5}O_{6-\delta}$ · Distribution relaxation times · Anode · Area-specific resistance · EIS · Symmetrical SOFC

Introduction

Conventional materials used for production of solid-state electrochemical devises (e.g., solid oxide fuel cells (SOFC), sensors, and electrolyzers) have some shortcomings, for example: low conductivity of doped zirconium oxide-based electrolytes (YSZ) at medium temperatures [1], interaction of lanthanum manganite-based cathodes with YSZ at high temperatures [2, 3], and degradation of Ni-based anodes [4, 5]. High operation temperatures of conventional SOFCs (near 900 °C) also have a negative influence on the stability of their components. Therefore, development of new materials for application in SOFCs is a significant trend.

Strontium ferrite-molybdate $Sr_2Fe_{1.5}Mo_{0.5}O_{6-\delta}$ (further SFM) are promising materials to be used as electrodes in intermedium temperature SOFCs. On the one hand, these materials are interesting because they may be simultaneously used as the oxygen (cathode) and fuel (anode) SOFC electrodes [6, 7], i.e., for symmetrical SOFC [8]. On the other hand, these materials have good stability, satisfactory electrical conductivity, and high electrochemical activity in reducing atmospheres [9–11], which makes them alternative to Ni/YSZ anodes.

Usually, to improve SFM properties, a heterovalent B-site doping was used. Thus, Sun et al. studied the iron substitution in SFM by Bi, Mg, and Al and demonstrated that the composition, in which 0.1 iron is substituted by bismuth, has the greatest electrical conductivity values [12]. The case when iron was replaced by nickel was studied in [13, 14] and it was shown that the addition of 0.1 of nickel into the iron sublattice had a positive influence on the anode performance.

✉ Denis A. Osinkin
OsinkinDA@mail.ru

[1] Institute of High-Temperature Electrochemistry, 20 Academicheskaya St., Yekaterinburg 620137, Russia

[2] Ural Federal University, 19 Mira St., Yekaterinburg 620002, Russia

[3] Institute of Solid State Chemistry, 91 Pervomayskaya St., Yekaterinburg 620990, Russia

The iron substitution in SFM by titanium [15], manganese [16], and copper [17] was also studied.

Therefore, heterovalent doping has a significant influence on the electronic balance in the oxide, which results in the conductivity improvement. Zhang et al. [18] demonstrated the influence of isovalent strontium substitution in $Sr_2FeMoO_{6-\delta}$ by barium and calcium and reported that in hydrogen atmosphere, the electrical conductivity increased in a Ba–Sr–Ca row. Huan et al. [19] also noted a positive influence of strontium substitution by calcium in strontium ferrite-molybdate. Dai et al. [20] illustrated that barium addition into the strontium sublattice changed SFM cathodes properties non-linearly. The electrical conductivity maximum was recorded for the $Sr_{1.8}Ba_{0.2}Fe_{1.5}Mo_{0.5}O_{6-\delta}$ composition. A further increase in barium concentration resulted in the conductivity decrease and electrochemical properties deterioration. The strontium substitution by calcium in the SFM cathode was studied by Qiao et al. [21]. The authors observed the maximum conductivity for the $Sr_{1.6}Ca_{0.4}Fe_{1.5}Mo_{0.5}O_{6-\delta}$ composition in air and TEC decrease at calcium concentration growth. Calcium-doped SFM electrodes have not been studied in reducing atmospheres.

We have previously studied SFM and SFM-SDC anodes in contact with the lanthanum gallate based electrolyte [22, 23] and have demonstrated that such anodes have high electrochemical activity in reducing medium, but their electrical conductivity is relatively small, about 12 S/cm at 800 °C. Also, we have previously studied the influence of strontium substitution by calcium in the $Sr_2MgMoO_{6-\delta}$ anodes [24] and have observed that the isovalent substitution caused a significant improvement in the anode performance. The aim of this study is to examine the effects of partial substitution of Ca for Sr on the functional and electrochemical properties of $Sr_{2-x}Ca_xFe_{1.5}Mo_{0.5}O_{6-\delta}$ as a fuel electrode.

Experimental

$Sr_{2-x}Ca_xFe_{1.5}Mo_{0.5}O_{6-\delta}$ powders preparation

$Sr_{2-x}Ca_xFe_{1.5}Mo_{0.5}O_{6-\delta}$ ($x = 0.05, 0.15, 0.3, 0.5$) powders, later Ca_xSFM, were synthesized using the citric route. $Sr(NO_3)_2$, $CaCO_3$, $Fe(NO_3)_3 \cdot 9H_2O$, $(NH_4)_6Mo_7O_{24} \cdot 4H_2O$, and $C_6H_8O_7 \cdot H_2O$ were used as initial reagents. First, calcium carbonate was dissolved in nitric acid until calcium nitrate formation. Then strontium, calcium, and iron nitrates were dissolved in distilled water, citric acid was added in the ratio 2:1. The ratio of citric acid to ammonium molybdate dissolution was 3:1. After that, the citrate solution of molybdenum was added to the strontium, calcium, and iron citrate solutions, which were continuously mixed. The transparent solution formed was evaporated on a hot stove. As a result, a porous mass was formed; at further heating, it started burning and powder-like agglomerates were formed. The obtained powders were grinded and calcined at 600 and 900 °C with final calcining at 1100 °C for 7 h in an alumina crucible with a closed lid.

Powders certification

The x-ray powder diffraction (XRD) study was carried out on a Rigaku D/MAX-2200 diffractometer using the Cu-Kα radiation ($\lambda = 1.5406$ Å) at room temperature in ambient air. The XRD patterns were recorded in the 2θ range of 10–70° with the step of 0.02 ° at the angular scanning rate of 4°/min. The crystalline structure of the powders was specified by the Rietveld method in the FullProf software [25].

TG and DSC measurements

Thermogravimetric measurements were carried out in 5% H_2/Ar with a Setaram Setsys Evolution thermoanalyzer with the accuracy exceeding 0.01 mg. In order to exclude the influence of undesirable moisture, the oxides were preliminarily heated in air up to 200 °C and kept at 200 °C for 2 h. Then, air was replaced by 5% H_2/Ar and after 30 min, the samples were heated with the heating rate of 7°/min and mass changes were recorded. DSC analysis was performed using a thermal analyzer STA 449F5 Jupiter produced by the NETZSCH company (Germany). The measurements were performed at heating in highly pure argon atmosphere with the heating rate of 10°/min in alumina crucibles.

Electrical and electrochemical measurements

To measure the conductivity, the samples were prepared in the form of bars using the uniaxial pressing (250 MPa) and were sintered at 1250 °C (100°/h) for 10 h in air. The obtained bars were about $20 \times 5 \times 5$ mm. After sintering, four Pt current wires were placed on the sample and then they were covered with Pt paste and sintered for 1 h at 950 °C in air. After the samples were assembled into the measuring rig, they were heated in air up to 800 °C; later, air was substituted by argon, then by 5% H_2/Ar and after that by wet (3% H_2O) hydrogen. The measurements were performed by the 4-probe DC method using FRA-1260 (Solartron).

To study the electrochemical performance of Ca_xSFM anodes, the symmetrical cells with the $La_{0.85}Sr_{0.15}Ga_{0.85}Mg_{0.15}O_3$ (LSGM) supporting electrolyte were made. The LSGM electrolyte preparation and certification are described in [26]. To prepare the electrode slurry, the Ca_xSFM powders were mixed with isopropyl alcohol and polyvinilbutirol. The electrode slurry was applied to the electrolyte by painting onto both sides. They were dried at 100 °C and calcined in air at 1050 °C for 2 h with the heating and cooling rates of 100°/h. After calcining, the electrodes thickness and area were about 30 μm and 0.3 cm², respectively. Buffer and current layers were not used. The

measuring rig and measurement setup are demonstrated in [27, 28], respectively. The area-specific polarization resistance (ASR) measurements were performed by means of the impedance spectroscopy in the frequency range of 100 kHz–0.01 Hz using a FRA-1260 and EI-1287 (Solartron). For the distribution of relaxation time (DRT) analysis, the program code, developed by the authors of [29] based on the Tikhonov's regularization [30], was applied. The Z-View software was used to analyze the impedance spectra by the non-linear least square method.

Solid oxide fuel cells (SOFC) of the planar design with the 1.5-mm-thick supporting LSGM electrolyte were analogously prepared. We tested both the symmetrical SOFC with $Ca_{0.15}SFM$ electrodes and that with the highly active 70 wt% $Pr_{0.9}Y_{0.1}BaCo_2O_{6-\delta}$ + 30 wt% SDC cathode [31] and Ca_xSFM ($x = 0.15$, 0.3) anodes. Both electrodes were simultaneously calcined at 1050 °C for 2 h in air. To determine the polarization losses at the cathode and anode across the supporting LSGM electrolyte perimeter, a Pt reference electrode was made and calcined at 950 °C for 1 h in air. The measurements of SOFC were performed under air/wet hydrogen condition. The SOFC performance data was recorded by means of the setup, described in [32].

SEM analysis

In order to obtain SEM images, the sample pores were filled with epoxy in vacuum and then the samples were polished by means of the Struers Labopol device. The SEM images of the anode were obtained by means of the electron microscope MIRA 3LMU. The analysis of the SEM images was performed using the ImageJ software. Figure 1 illustrates the electrode layer thickness. The porosity of electrodes obtained from SEM images was about 44–48%.
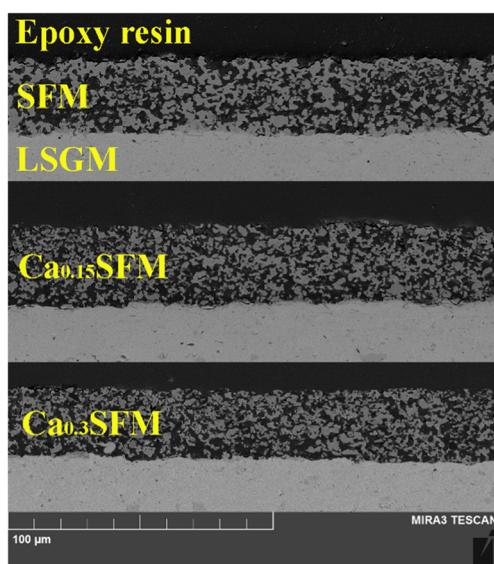

Fig. 1 SEM images of the LSGM electrolyte/$Sr_{2-x}Ca_xFe_{1.5}Mo_{0.5}O_{6-\delta}$ electrode cross-section

Results and discussion

Powders characterization

Figure 2 demonstrates XRD patterns with (hkl) reflections of Ca_xSFM powders with different calcium content. It also illustrates XRD patterns of the compositions with 0.15 and 0.5 calcium after reducing calcining at 900 °C for 17 h in 5% H_2/Ar. Phase analysis of the powders showed that after synthesis, the obtained oxides apart from $Ca_{0.5}SFM$ had a single-phase structure. Reflexes of the admixture phases were observed for the composition with 0.5 calcium content in the angular range of $25° < 2\theta < 33°$. The impurity phase was identified as $SrFe_2O_5$ (JCPDS 37-1320). It should be mentioned that the formation of admixture phases with the increase in calcium content in Ca_xSFM was reported in [21]. After the reducing sintering the small intensity reflexes, which correspond to the iron phase (JCPDS 06-0696), were observed on the XRD patterns. Such behavior is frequently observed in the ferrite-molybdate anodes [23, 33]. The admixture phases apart from iron admixtures were observed in the narrow-angle region of the $Ca_{0.5}SFM$ composition, which is why we did not study this composition further.

Rietveld refinement of the powder x-ray diffraction data for Ca_xSFM converges to a satisfactory solution in space group $Pm-3m$ of the cubic system (Table 1). The total convergence parameter χ^2 was in the range 2.16–4.19. The obtained results indicate that at the isovalent substitution of strontium by calcium the crystalline lattice parameter decreases monotonously.

After the reducing treatment of the $Ca_{0.15}SFM$ powder (5%H_2/Ar 900 °C), the crystalline lattice parameter calculated
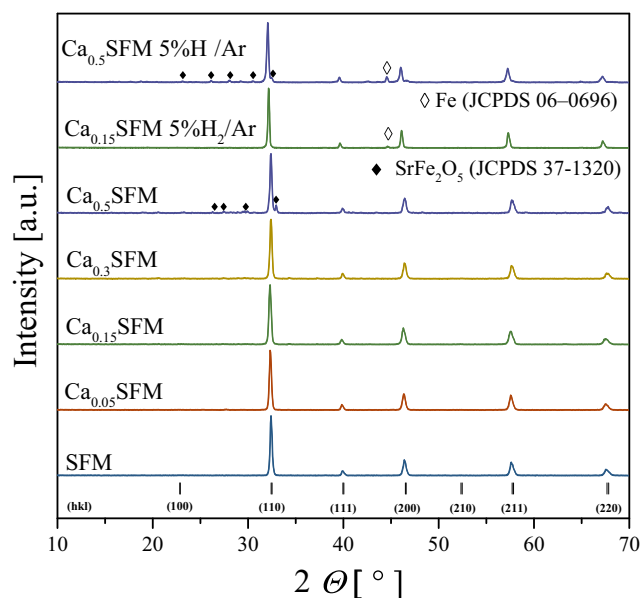

Fig. 2 XRD patterns of as-prepared in air at 1100 °C $Sr_{2-x}Ca_xFe_{1.5}Mo_{0.5}O_{6-\delta}$ ($x = 0$, 0.05, 0.15, 0.3, 0.5) and after reduction at 900 °C for 17 h in 5% H_2/Ar, marks indicate the impurity phases

Table 1 Structural refinement results

Composition	a (Å)	Rp (%)	Rwp (%)	χ^2
SFM	3.9227 (6)	5.1	11.6	2.16
Ca$_{0.05}$SFM	3.9221 (9)	4.6	12.4	2.29
Ca$_{0.15}$SFM	3.9213 (4)	4.7	10.9	2.6
Ca$_{0.3}$SFM	3.9186 (5)	4.8	11.2	2.84
Ca$_{0.5}$SFM	3.9171 (1)	8.3	14.5	4.19
Ca$_{0.15}$SFM red	3.9327 (5)	8.1	12.9	4.09

according to the Rietveld method was 3.9327(5) Å, whereas it was equal to 3.9213(4) Å after the synthesis in air. This is due to the release of oxygen from the lattice, which results in the expansion of the crystal lattice.

DSC and TG analysis

The DSC analysis (Fig. 3a) of all samples in high-purity argon signified a similar regularity, i.e., at the temperature growth the DSC signal shifted to the exothermal area. The minimum was observed at 700 °C for the Ca$_{0.15}$SFM and Ca$_{0.3}$SFM compositions. It is complicated to explain such behavior; however, we assume that it may be associated with a gradual powder calcining at the temperature growth. Absence of peaks on the DSC curves illustrate that there are no phase transitions in the studied oxides at the temperature growth in argon. It should be noted that Cowin et al. [33] also reported on the absence of phase transitions in Sr$_{1.6}$K$_{0.4}$Fe$_{1+x}$Mo$_{1-x}$O$_{6-\delta}$ ($x =$ 0.2, 0.4, 0.6) but in reducing medium.

TG analysis of the powders was performed in 5% H$_2$/Ar at 900 °C. First, the samples were slowly heated in air up to 200 °C and were exposed for 2 h to remove moisture traces from the powders. Then, while the temperature was maintained air was substituted by 5% H$_2$/Ar and after a complete blow-off, which continued during half an hour, the samples were heated to 900 °C, the data was recorded, and the samples were exposed for 17 h at 900 °C. Figure 3b demonstrates that in reducing medium, the TG curve has several steps. The first one is from 200 to 400 °C, it has the greatest inclination and it is associated with the oxygen removal from the perovskite crystalline lattice. The further weight change is probably accompanied with the oxygen removal and iron ion reduction. In reducing atmosphere as opposed to argon atmosphere, a clear correlation between the powder weight change and the calcium content is observed. As the calcium content increases, the Δm increases. During the isothermal exposure for 17 h at 900 °C, the weight changed insignificantly and the process of saturation started. In [16] data on the TG measurements of the SFM powder of about 2% mass change in 5% H$_2$/Ar at 800 °C was obtained.
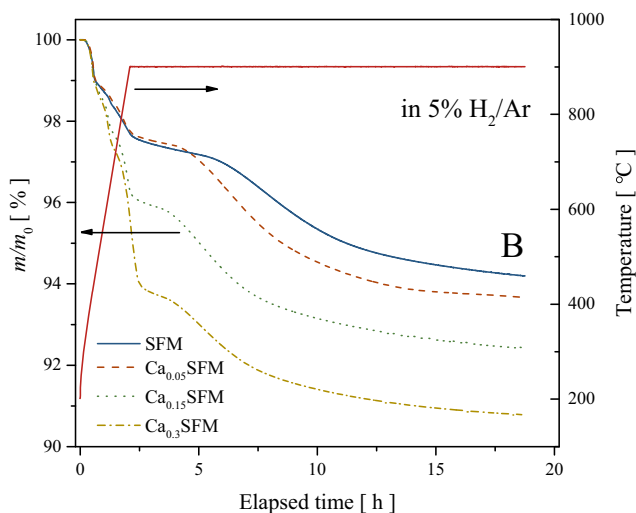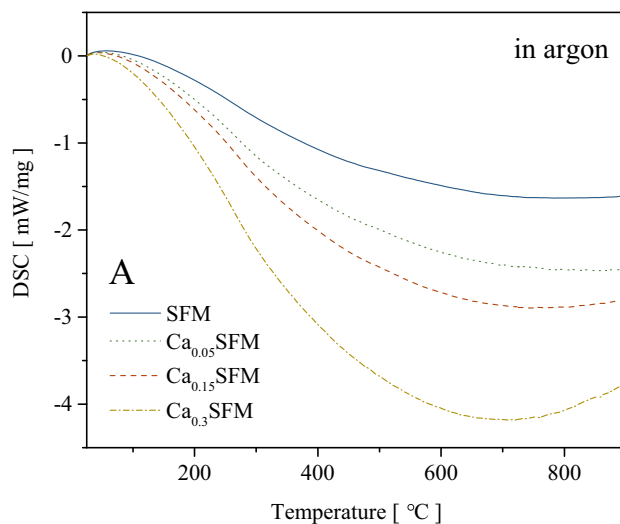

Fig. 3 (**a**) DSC analysis in high-purity argon. (**b**) TG dependencies in 5% H$_2$/Ar

Measurements of total conductivity under reducing conditions

Total conductivity was studied using the compact samples by the four-probe DC method in wet (3% H$_2$O) hydrogen in the temperature range of 600–800 °C. The results are illustrated in Fig. 4. It is seen that the obtained dependencies in the Arrhenius plot have a thermoactive (semi-conductive) behavior. For the non-doped composition, the electrical conductivity values are within the 10–15 S/cm range, which is in agreement with data [9, 34]. In the 0–0.05–0.15 calcium concentration row, the electrical conductivity increases as the dopant concentration grows with the maximum value of about 33 S/cm for Ca$_{0.15}$SFM at 800 °C. At a further decrease in the calcium concentration, the insignificant decrease in conductivity was observed. Authors [21] also reported on the non-linear dependence of Ca$_x$SFM conductivity at calcium content increase,

	600 C	700 C	800 C
SFM	10.5	12.8	15.2
Ca0.05SFM	19.2	21.5	23.4
Ca0.15SFM	26.2	29.5	33.1
Ca0.3SFM	23.8	26.4	29.1

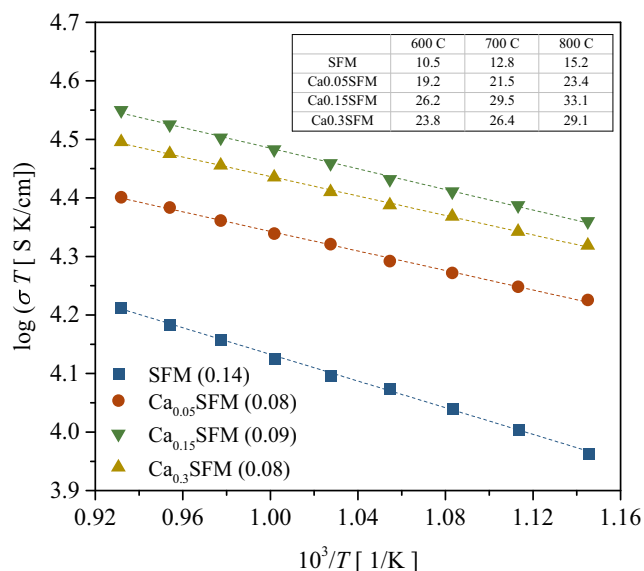Legend: ■ SFM (0.14); ● Ca$_{0.05}$SFM (0.08); ▼ Ca$_{0.15}$SFM (0.09); ▲ Ca$_{0.3}$SFM (0.08)

Fig. 4 Total conductivity of samples in wet hydrogen, activation energies (eV) are given in parentheses. The conductivity values (S/cm) are given in inserted table

but only in oxidation atmosphere. The total conductivity of ferrite-molybdates in reducing atmosphere is composed of two types of conductivity: oxygen-ionic and electronic, which is realized by means of small polaron hopping mechanism that occurs through the red-ox reaction $Fe^{3+} + Mo^{5+} = Fe^{2+} + Mo^{6+}$. Taking into account the low values of oxygen-ionic conductivity of ferrite-molybdates [34], their total electrical conductivity is completely defined by the small polaron hopping mechanism, which is testified by low activation energies of total electrical conductivity of about 0.1 eV (Fig. 4).

Due to the fact that this work is aimed at the study of the isovalent doping influence, the dopant concentration increase does not influence the electron balance in the crystal and oxygen vacancies concentration. Though the strontium substitution by calcium leads to the lattice parameter decrease (Table 1), and as a result to the decrease in the bound length in the crystal, which causes the conductivity increase in reducing atmosphere by the small polaron hopping. As the described mechanism is realized by means of the $Fe^{3+} + Mo^{5+} = Fe^{2+} + Mo^{6+}$ reaction the red-ox Fe^{2+}/Mo^{6+} and Fe^{3+}/Mo^{5+} couples relation influence is great. In [21], authors report that red-ox pairs optimal relation is characteristic of the composition with small calcium concentration. Further calcium concentration increase the conductivity value will decrease, which is seen in Fig. 4 (inserted table).

Electrochemical measurements

The electrochemical impedance was used to study the area-specific resistance (ASR) of the Ca$_x$SFM electrodes at the equilibrium potential in wet hydrogen using symmetrical electrochemical cells with the LSGM-supporting electrolyte.

Impedance spectra of the Ca$_{0.15}$SFM/LSGM/Ca$_{0.15}$SFM cell at various temperatures are exemplified in Fig. 5. The serial resistance was substantially subtracted from the spectra for a better visual perception. Figure 5 demonstrates that impedance spectra have a complex form without clear separation of semicircles, which testifies that hydrogen electro-oxidation is a multistage process and that there are several rate-determining stages.

Figure 6 illustrates the ASR temperature dependencies, which were calculated from spectra. The obtained values are seen to be below 1 Ω cm^2 in the 800–650 °C temperature range. In addition, there is a direct dependence between ASR and anode electrical conductivity. The minimum ASR was obtained for the Ca$_{0.15}$SFM composition, which is 0.12 Ω cm^2 at 800 °C. It should be noted that the obtained ASR temperature dependencies are non-linear in the Arrhenius plot, i.e., there is an inclination decrease in high-temperature region. Probably, this is due to gas-diffusion processes, which appear at the temperature growth and which have a thermal deactivation behavior, i.e., the resistance of this stage increases as the temperature grows [27, 35]. To prove the assumption on the gas diffusion influence on the anodes characteristics, the impedance spectra were measured, when current passed through the neighboring samples, which permitted to decrease or remove completely the gas diffusion stage influence. Such approach was used before at the studies of the Ni-based anodes and it is described in detail in [27]. Indeed, when the electric current connection is made through the sample, the low-frequency part of the spectrum disappears (Fig. 5).

The DRT curves, illustrated in Fig. 7, were calculated to analyze the impedance spectra at the first stage. It is obvious that the electrochemical reaction is limited by three rate-
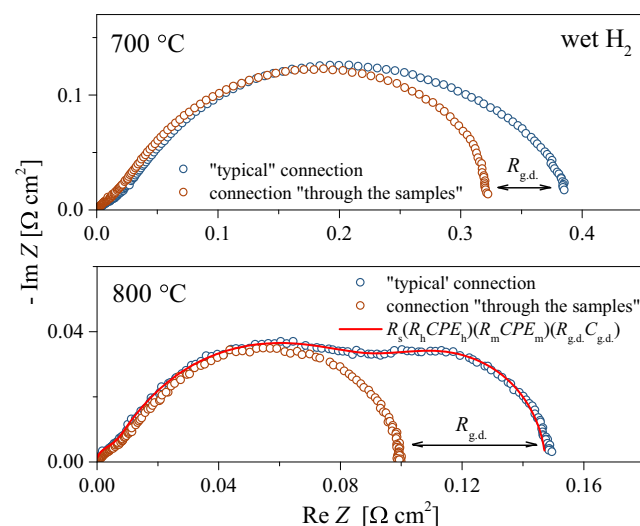

Fig. 5 Impedance spectra of the Ca$_{0.15}$SFM/LSGM/Ca$_{0.15}$SFM cell at various temperatures and different method of cell connection in wet hydrogen
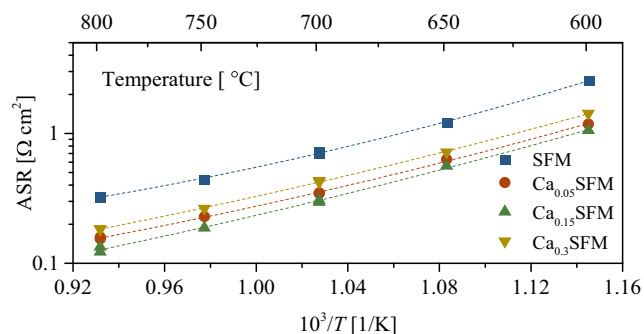
Fig. 6 Temperature dependencies of the anode area specific resistances (ASR) in wet hydrogen

Fig. 8 Temperature dependencies of partial polarization resistances in wet hydrogen

determining stage: high-frequency one with the frequency maximum near 500 Hz, mid-frequency one with the frequency of about 5 Hz, and low-frequency one. In addition, the DRT curves, which were calculated using the impedance spectra, obtained at a normal samples connection and a connection through the sample, also demonstrated that when the samples were connected "through the sample" the low-frequency process disappeared completely.

On the basis of the data obtained from DRT curves, i.e., a number of the rate-determining steps, the impedance spectra were fitted by the least square method using the equivalent scheme: $R_s(R_h CPE_h)(R_m CPE_m)(R_{g.d.} C_{g.d})$, where R_s is the subsequent resistant, R is the partial polarization resistance, and CPE is the constant phase element. The fitting spectrum is demonstrated in Fig. 5 by a solid line and the temperature dependence of partial polarization resistances is presented in Fig. 8.

It is seen that the high-frequency resistance does not depend on the calcium concentration; in addition, it is worth mentioning a poor detection accuracy and insignificant impact to the anode ASR. Taking into account frequencies at which this stage is recorded, i.e., near 500 Hz, the charge transport stage is not the rate-determining one. This process may be related to the contact resistances at the electrode/electrolyte border. The mid-frequency resistance depends on the calcium content the same way as ASR. In addition, the minimum R_m value was observed at the calcium concentration of 0.15. He
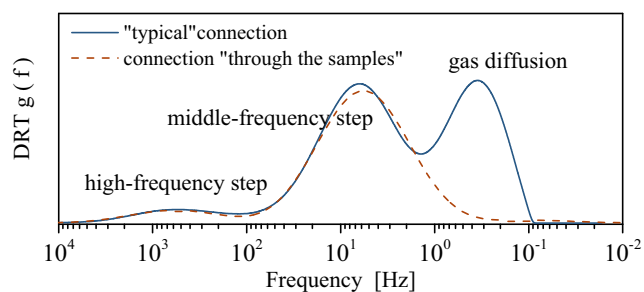
et al. [34] reported that the partial polarization resistance in the SFM anode, which was recorded at about 2 Hz, is related with the oxygen ion transport in the anode. The strontium substitution by calcium results in the lattice parameter decrease and, therefore, in the decrease in the connection length, which increases supposedly the ionic conductivity. Thus, the strontium substitution by calcium provokes the decrease in the partial process resistance, which takes place at the oxygen ion transport in the anode. Such behavior is observed in Fig. 8. The mid-frequency stage activation energy is within 0.9–1 eV (no direct correlation between the activation energy and calcium concentration was observed), which is in agreement with the above stated hypothesis on the nature of the mid-frequency stage. The low-frequency resistance is not thermoactive and does not depend on the calcium concentration in the anode, which confirms the gas-diffusion nature.

SOFCs performance

The study of Ca$_x$SFM as a SOFC electrode was performed using a planar cell with the 1.5-mm-thick supporting LSGM electrolyte. Three types of cells were studied. In two cells, a previously synthesized, certified, and tested composite of 70 wt% Pr$_{0.9}$Y$_{0.1}$BaCo$_2$O$_{6-\delta}$ + 30 wt% SDC (PYBC + SDC) was used as a cathode [31] and in the third cell, symmetrical Ca$_{0.15}$SFM electrodes were applied. Figure 9 shows the test results of the fuel cells. When air was used as the oxidizer and wet hydrogen was used as fuel all studied SOFCs had close power density values at 800 °C. The largest power density of about 0.18 W/cm^2 was obtained for the cell with the PYBC + SDC cathode and the Ca$_{0.15}$SFM anode. Other cells had similar power density values of 0.15 W/cm^2.

Usage of the thick electrolyte allowed fabricating a reference electrode for the cathode and anode overvoltage

Fig. 7 DRT curves calculated from spectra of the Ca$_{0.15}$SFM/LSGM/Ca$_{0.15}$SFM cell at 800 °C

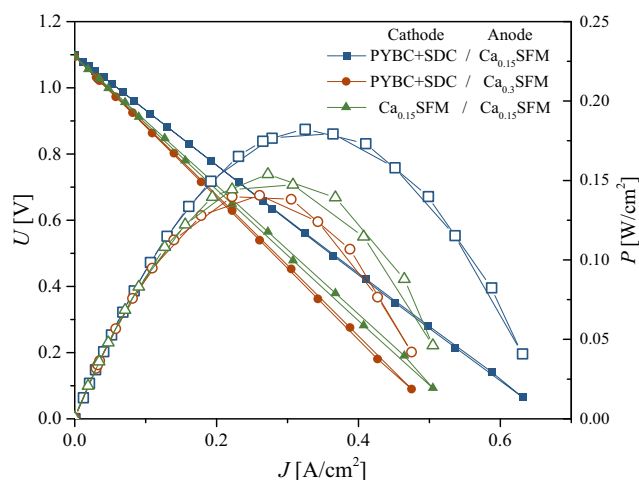**Fig. 9** *I–U* and *I–P* curves of different SOFCs at 800 °C under air/humid hydrogen condition

detection. Figure 10 presents the obtained results. The composite PYBC + SDC cathode demonstrated low overvoltage, which did not exceed 0.1 V at the current density of 1 A/cm^2, which is close to the previously obtained results for symmetrical cells with analogous electrodes in contact with the SDC electrolyte (dotted line, Fig. 10) [31]. The Ca$_{0.15}$SFM anode overvoltage was also sensibly low, about 0.12 V at the current density of 1 A/cm^2. The anode of the Ca$_{0.3}$SFM composition had an unsurprisingly noticeably worse result, due to the lower electrical conductivity and polarization resistance values. The Ca$_{0.15}$SFM cathode overvoltage was predictably higher as compared to that of the PYBC + SDC cathode, because of the low rates of hetero exchange of ferrite-molybdate cathode with oxygen [36, 37].
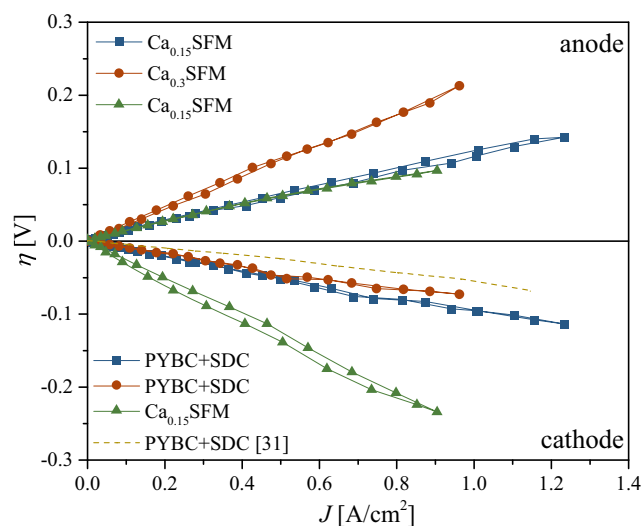

Fig. 10 Cathode and anode overvoltage of different SOFCs at 800 °C under air/wet hydrogen conditions

Conclusions

Ca-doped strontium ferrite-molybdates Sr$_{2-x}$Ca$_x$Fe$_{1.5}$Mo$_{0.5}$O$_{6-\delta}$ ($x = 0$, 0.05, 0.15, 0.3, 0.5) have been studied under reducing conditions. The strontium substitution by calcium to $x = 0.3$ inclusive did not result in formation of any admixture phases in oxides. A good stability and absence of oxide phase transitions in argon in the temperature range of 25–900 °C as well as an insignificant decrease in weight at 900 °C in 5% H$_2$/Ar were observed. A non-linear dependence of electrical and electrochemical characteristics on calcium concentration is shown. Taking into account a satisfactory electrical conductivity of about 33 S cm^{-1}, low ASR value of about 0.12 Ω cm^2, good stability in reducing medium and low anode overvoltage during SOFC operation, about 0.12 V at 1 A cm^2 at 800 °C, Sr$_{1.85}$Ca$_{0.15}$Fe$_{1.5}$Mo$_{0.5}$O$_{6-\delta}$ may be recommended as a perspective anode material for medium-temperature solid oxide fuel cells.

Publisher's Note Springer Nature remains neutral with regard to jurisdictional claims in published maps and institutional affiliations.

References

1. Irvine JTS, Connor P (2013) Solid oxide fuels cells: facts and figures. Springer-Verlag, London
2. Yang CT, Wei WJ, Roosen A (2004) Reaction kinetics and mechanisms between La$_{0.65}$Sr$_{0.3}$MnO$_3$ and 8 mol% yttria-stabilized zirconia. J Am Ceram Soc 87(6):1110–1116
3. Wiik K, Schmidt CR, Faaland S, Shamsili S, Einarsrud M, Grande T (1999) Reactions between strontium-substituted lanthanum manganite and yttria-stabilized zirconia: I, powder samples. J Am Ceram Soc 82:721–728
4. Hauch A, Mogensen M (2010) Ni/YSZ electrode degradation studied by impedance spectroscopy: effects of gas cleaning and current density. Solid State Ionics 181(15-16):745–753
5. Osinkin DA, Kuzin BL, Bogdanovich NM (2013) Time dependence of electrochemical characteristics of high performance CeO$_2$-modified Ni-cermet electrode in multicomponent gas mixtures H$_2$ + H$_2$O + CO + CO$_2$. Solid State Ionics 251:66–69
6. Liu Q, Dong X, Xiao G, Zhao F, Chen F (2010) A novel electrode material for symmetrical SOFCs. Adv Mater 22(48):5478–5482

7. Osinkin DA, Beresnev SM, Lobachevskaya NI (2017) Symmetrical solid oxide fuel cell with strontium ferrite-molybdenum electrodes. Russ J Electrochem 53(6):665–669

8. Ruiz-Morales JC, Marrero-Lopez D, Canales-Vazquezc J, Irvine JTS (2011) Symmetric and reversible solid oxide fuel cells. RSC Adv 1(8):1403–1414

9. Miao G, Yuan C, Chen T, Zhou Y, Zhan W, Wang S (2016) $Sr_2Fe_{1+x}Mo_{1-x}O_{6-\delta}$ as anode material of cathode-supported solid oxide fuel cells. Int J Hydrog Energy 41(2):1104–1111

10. Feng J, Yang G, Dai N, Wang Z, Sun W, Rooney D, Qiao J, Sun K (2014) Investigation into the effect of Fe-site substitution on the performance of $Sr_2Fe_{1.5}Mo_{0.5}O_{6-\delta}$ anodes for SOFCs. J Mater Chem A 2:17628–17634

11. Hou M, Sun W, Li P, Feng J, Yang G, Qiao J, Wang Z, Rooney D, Feng J, Sun K (2014) Investigation into the effect of molybdenum-site substitution on the performance of $Sr_2Fe_{1.5}Mo_{0.5}O_{6-\delta}$ for intermediate temperature solid oxide fuel cells. J Power Sources 272: 759–765

12. Sun K, Liu J, Feng J, Yuan H, He M, Xu C, Wang Z, Sun W, Qiao J (2017) Investigation of B-site doped perovskites $Sr_2Fe_{1.4}X_{0.1}Mo_{0.5}O_{6-\delta}$ (X=Bi, Al, Mg) as high-performance anodes for hybrid direct carbon fuel cell. J Power Sources 365:109–116

13. Feng J, Qiao J, Wang W, Wang Z, Sun W, Sun K (2016) Development and performance of anode material based on A-site deficient $Sr_{2-x}Fe_{1.4}Ni_{0.1}Mo_{0.5}O_{6-\delta}$ perovskites for solid oxide fuel cells. Electrochim Acta 215:592–599

14. Xiao G, Wang S, Lin Y, Yang Z, Han M, Chen F (2014) Ni-doped $Sr_2Fe_{1.5}Mo_{0.5}O_{6-\delta}$ as anode materials for solid oxide fuel cells. J Electrochem Soc 161(3):F305–F310

15. Zhou Q, Cheng Y, Li W, Yang X, Liu J, An D, Tong X, Zhong B, Wang W (2016) Investigation of cobalt-free perovskite $Sr_2FeTi_{0.75}Mo_{0.25}O_{6-\delta}$ as new cathode for solid oxide fuel cells. Mater Res Bull 74:129–133

16. Zheng K, Swierczek K, Polfus JM, Sunding MF, Pishahang M, Norby T (2015) Carbon deposition and sulfur poisoning in $SrFe_{0.75}Mo_{0.25}O_{3-\delta}$ and $SrFe_{0.5}Mn_{0.25}Mo_{0.25}O_{3-\delta}$ electrode materials for symmetrical SOFCs. J Electrochem Soc 162(9):F1078–F1087

17. Wang S, Hsu Y, Huang M, Chang C, Cheng S (2016) Characteristics of copper-doped $SrFe_{0.75}Mo_{0.25}O_{3-\delta}$ ceramic as a cathode material for solid oxide fuel cells. Solid State Ionics 296: 120–126

18. Zhang L, Zhou Q, He Q, He T (2010) Double-perovskites $A_2FeMoO_{6-\delta}$ (A = Ca, Sr, Ba) as anodes for solid oxide fuel cells. J Power Sources 195(19):6356–6366

19. Huan Y, Li Y, Yin B, Ding D, Wei T (2017) High conductive and long-term phase stable anode materials for SOFCs: A_2FeMoO_6 (a = Ca, Sr, Ba). J Power Sources 359:384–390

20. Dai N, Wang Z, Jiang T, Feng J, Sun W, Qiao J, Rooney D, Sun K (2014) A new family of barium-doped $Sr_2Fe_{1.5}Mo_{0.5}O_{6-\delta}$ perovskites for application in intermediate temperature solid oxide fuel cells. J Power Sources 268:176–182

21. Qiao J, Chen W, Wang W, Wang Z, Sun W, Zhang J, Sun K (2016) The Ca element effect on the enhancement performance of $Sr_2Fe_{1.5}Mo_{0.5}O_{6-\delta}$ perovskite as cathode for intermediate-temperature solid oxide fuel cells. J Power Sources 331:400–407

22. Osinkin DA, Lobachevskaya NI, Kuzmin AV (2017) Transport and electrochemical properties of $Sr_2Fe_{1.5}Mo_{0.5}O_6 + Ce_{0.8}Sm_{0.2}O_{1.9}$ composite as promising anode for solid oxide fuel cells. Russ J Appl Chem 90(1):41–46

23. Osinkin DA, Lobachevskaya NI, Suntsov AY (2017) The electrochemical behavior of the promising $Sr_2Fe_{1.5}Mo_{0.5}O_{6-\delta} + Ce_{0.8}Sm_{0.2}O_{1.9-\delta}$ anode for the intermediate temperature solid oxide fuel cells. J Alloys Comp 708:451–455

24. Osinkin DA, Zabolotskaya EV, Kellerman DG, Suntsov AY (2018) The physical properties and electrochemical performance of Ca-doped $Sr_2MgMoO_{6-\delta}$ as perspective anode for solid oxide fuel cells. J Solid State Electrochem 22(4):1209–1215

25. Rietveld HM (1969) A profile refinement method for nuclear and magnetic structures. J Appl Crystallogr 2(2):65–71

26. Osinkin DA, Lobachevskaya NI, Bogdanovich NM (2017) Effect of the copper oxide sintering additive on the electrical and electrochemical properties of anode materials based on $Sr_2Fe_{1.5}Mo_{0.5}O_{6-\delta}$. Russ J Appl Chem 90(10):1686–1692

27. Osinkin DA, Kuzin BL, Bogdanovich NM (2009) Gas diffusion hindrances on Ni cermet anode in contact with $Zr_{0.84}Y_{0.16}O_{1.92}$ solid electrolyte. Russ J Electrochem 45(4):483–489

28. Osinkin DA (2016) Long-term tests of $Ni-Zr_{0.9}Sc_{0.1}O_{1.95}$ anode impregnated with CeO_2 in $H_2 + H_2O$ gas mixtures. Int J Hydrog Energy 41(39):17577–17584

29. Gavrilyuk AL, Osinkin DA, Bronin DI (2017) The use of Tikhonov regularization method for calculating the distribution function of relaxation times in impedance spectroscopy. Russ J Electrochem 53(6):575–588

30. Tikhonov AN, Arsenin VY (1977) Solution of ill-posed problems. Winston & Sons, Washington

31. Marshenya SN, Politov BV, Osinkin DA, Suntsov AY, Kozhevnikov VL (2018) Functional properties and electrochemical performance of dual-phase $Pr_{0.9}Y_{0.1}BaCo_2O_{6-\delta}–Ce_{0.8}Sm_{0.2}O_{1.9}$ composite cathodes. J Solid State Electrochem 22(6):1863–1869

32. Beresnev SM, Bobrenok OF, Kuzin BL, Bogdanovich NM, Kurteeva AA, Osinkin DA, Vdovin GK, Bronin DI (2012) Single fuel cell with supported LSM cathode. Russ J Electrochem 48(10): 969–975

33. Cowin PI, Lan R, Petit CTG, Wang H, Tao S (2016) Conductivity and redox stability of new double perovskite oxide $Sr_{1.6}K_{0.4}Fe_{1+x}Mo_{1-x}O_{6-\delta}$ (x = 0.2, 0.4, 0.6). J Mater Sci 51(8):4115–4124

34. He B, Zhao L, Song S, Liu T, Chen F, Xia C (2012) $Sr_2Fe_{1.5}Mo_{0.5}O_{6-\delta}–Sm_{0.2}Ce_{0.8}O_{1.9}$ composite anodes for intermediate-temperature solid oxide fuel cells. J Electrochem Soc 159(5):B619–B626

35. Osinkin DA, Bogdanovich NM, Gavrilyuk AL (2016) Rate determining steps of fuel oxidation over CeO_2 impregnated Ni-YSZ in $H_2 + H_2O + CO + CO_2$ ambient. Electrochim Acta 199:108–115

36. Wang Y, Hu B, Zhu Z, Boumeester HJM, Xia C (2014) Electrical conductivity relaxation of $Sr_2Fe_{1.5}Mo_{0.5}O_{6-\delta}–Sm_{0.2}Ce_{0.8}O_{1.9}$ dual-phase composites. J Mater Chem A 2(1):136–143

37. Osinkin DA, Beresnev SM, Bogdanovich NM (2018) Influence of Pr_6O_{11} on oxygen electroreduction kinetics and electrochemical performance of $Sr_2Fe_{1.5}Mo_{0.5}O_{6-\delta}$ based cathode. J Power Sources 392:41–47